

High-efficiency ultra-fast all-optical photonic crystal diode based on the lateral-coupled nonlinear elliptical defect

Daxing Li(李大星), Kaizhu Liu(刘凯柱), Chunlong Yu(余春龙), Kuo Zhang(张括), Yueqin Liu(刘跃钦), and Shuai Feng(冯帅)

Citation: Chin. Phys. B, 2024, 33 (**3**): 034215. DOI: 10.1088/1674-1056/ad0117
Journal homepage: http://cpb.iphy.ac.cn; http://iopscience.iop.org/cpb

What follows is a list of articles you may be interested in

Enhanced and controllable reflected group delay based on Tamm surface plasmons with Dirac semimetals

Qiwen Zheng(郑棋文), Wenguang Lu(卢文广), Jiaqing Xu(胥加青),Yunyang Ye(叶云洋), Xinmin Zhao(赵新民), and Leyong Jiang(蒋乐勇)

Chin. Phys. B, 2023, 32 (**7**): 074208. DOI: 10.1088/1674-1056/aca205

High-performance chiral all-optical OR logic gate based on topological edge states of valley photonic crystal

Xiaorong Wang(王晓蓉), Hongming Fei(费宏明), Han Lin(林瀚), Min Wu(武敏), Lijuan Kang(康丽娟), Mingda Zhang(张明达), Xin Liu(刘欣), Yibiao Yang(杨毅彪), and Liantuan Xiao(肖连团)

Chin. Phys. B, 2023, 32 (**7**): 074205. DOI: 10.1088/1674-1056/accb41

Dynamic light storage based on controllable electromagnetically induced transparency effect

Liu-Ying Zeng(曾柳莹), Jun-Fang Wu(吴俊芳), and Chao Li(李潮)

Chin. Phys. B, 2023, 32 (**6**): 064213. DOI: 10.1088/1674-1056/acd2bd

Size effect on light propagation modulation near band edges in one-dimensional periodic structures

Yang Tang(唐洋), Jiajun Wang(王佳俊), Xingqi Zhao(赵星棋), Tongyu Li(李同宇), and Lei Shi(石磊)

Chin. Phys. B, 2023, 32 (**5**): 054201. DOI: 10.1088/1674-1056/acac0d

Spontaneous emission from Λ-type three-level atom driven by bichromatic field in anisotropic double-band photonic crystals

Kai Ling(凌凯), Li Jiang(姜丽), Ren-Gang Wan(万仁刚), and Zhi-Hai Yao(姚治海)

Chin. Phys. B, 2023, 32 (**4**): 044211. DOI: 10.1088/1674-1056/aca39b

---

High-efficiency ultra-fast all-optical photonic crystal diode based on the lateral-coupled nonlinear elliptical defect

Daxing Li(李大星)[1,2,3], Kaizhu Liu(刘凯柱)[4], Chunlong Yu(余春龙)[1,2,3], Kuo Zhang(张括)[1,2,3], Yueqin Liu(刘跃钦)[1,2,3], and Shuai Feng(冯帅)[1,2,3,†]

[1] *School of Science, Minzu University of China, Beijing* 100081, *China*
[2] *Optoelectronics Research Center, Minzu University of China, Beijing* 100081, *China*
[3] *Engineering Research Center of Photonic Design Software, Ministry of Education, Beijing* 100081, *China*
[4] *School of Optoelectronic Engineering and Instrumentation Science, Dalian University of Technology, Dalian* 116024, *China*

(Received 1 August 2023; revised manuscript received 24 September 2023; accepted manuscript online 7 October 2023)

An all-optical Fano-like diode featuring a nonlinear lateral elliptical micro-cavity and a reflecting column in the photonic crystal waveguide is proposed. The asymmetric micro-cavity is constructed by removing one rod and changing the shape of the lateral rod from a circle to an ellipse. A reflecting pillar is also introduced into the waveguide to construct an F–P cavity with the elliptical defect and enhance the asymmetric transmission for the incident light wave transmitting rightwards and leftwards, respectively. By designing the size of the ellipse and optimizing a reflecting rod at a suitable position, a maximum forward light transmittance of −1.14 dB and a minimum backward transmittance of −57.66 dB are achieved at the working wavelength of 1550.47 nm. The corresponding response time is about 10 ps when the intensity of the pump light beam resonant at 637 nm is 3.97 W/μm^2.

Keywords: photonic crystal, all-optical diode, Fano cavity, unidirectional transmission

PACS: 42.70.Qs, 42.25.Bs, 78.67.Pt **DOI:** 10.1088/1674-1056/ad0117

1. Introduction

All-optical devices have significant applications in the fields of optical communication, quantum computing, etc. A photonic crystal (PhC) is an artificial structure composed of two or more materials with different dielectric constants arranged periodically in space.[1,2] In PhCs, it is well known that the absence of transmission is mostly the consequence of the presence of photonic band gaps [frequency ranges of the forbidden (not allowed) modes].[3] The photonic band gap can be applied to achieve near-perfect reflection[4,5] and sophisticated modulation[6,7] of light polarization. An important feature of PhCs is photon localization. When the periodic structure of the PhC is disrupted, a defect mode is stimulated within the photonic band gap, causing photons at, particular frequencies, to be localized within the defect region, while photons with frequencies deviating from the defect mode will be strongly scattered. Based on the photon localization property of PhCs, various optical devices have been developed, such as switches,[8–12] beam splitters,[13–15] diodes[16–28] and logic gates.[29–32]

All-optical diodes (AODs) allow the light beam to propagate along one direction, while the opposite directional transmission is blocked. Many kinds of AODs have been achieved through using magnetic-optical materials, optical nonlinear effects, chiral metamaterials, etc. In 1994, Scalora *et al.* proposed a nonlinear PhC AOD.[16] For different incident directions, there is a pronounced contrast between the spatial electric field distributions near the bandgap edge since the bandgap position varies with the medium's refractive index and the medium's refractive index varies with light intensity. One-way transmission can be achieved by using the band-gap edge as the working wavelength and employing the bandgap's displacements for different incident directions. However, AODs leveraging band gaps have limitations since PhCs only have two top and bottom bandgap edges, restricting the working wavelength to the bandgap edge and narrowing the AOD's applicability. This led to researchers focusing more on AODs composed of PhC defects. In 2014, Bulgakov *et al.* introduced an AOD based on Kerr micro-cavity dipole modes in an asymmetric L-shaped PhC waveguide, and a response time of approximately 177 fs with 90% forward transmittance was achieved.[17] In 2016, Liu *et al.* proposed a high-efficiency AOD based on a PhC waveguide.[18] This AOD attained a response time of around 50 ps with approximately 75% forward transmittance. In 2017, Sato *et al.* presented a high-forward-transmission AOD based on a cascaded side-coupled PhC L3-type micro-cavity.[19] This AOD achieved a response time of about 250 ps with a forward transmittance of 99.8% and a reverse transmittance of −53 dB, thereby improving forward and reverse transmission contrast, although it resulted in increased response time.

Nonlinear PhCs are among the most promising structural types for designing AODs, due to their small size and low power requirements. In this paper, we have designed a

†Corresponding author. E-mail: fengshuai75@163.com

© 2024 Chinese Physical Society and IOP Publishing Ltd

high-transmittance, short-response-time AOD based on a two-dimensional (2D) square-lattice PhC structure. The structure consists of a W1-type channel, an asymmetric point defect, an elliptical side-coupling cavity and a reflection pillar. By changing the intensity of the pump light, this structure controls forward propagation and reverse cut-off of the signal light within the PhC structure. It also reduces the response time to a certain extent while maintaining high transmittance contrast for forward and reverse propagation.

2. Structure design

In this paper, we designed a 2D square lattice PhC structure consisting of dielectric rods immersed in an air background, whose refractive index is set at 3.1 for the near-infrared wavelength of around 1550 nm. The lattice constant of the PhC $a = 600$ nm, and the radius of the pillars $r = 0.2a$. We used the finite-difference time-domain (FDTD) method to calculate the band structure diagram of the perfect PhC [in Fig. 1(a)], the light transmission and spatial electric field distribution through the finite PhC structure. The TM-polarized mode is selected as the incident light, whose electric field distribution is parallel to the central axis of the pillar. As shown in Fig. 1(b), the photonic band gap of the afore-mentioned PhC ranges from 0.312 a/λ to 0.437 a/λ. When one row of pillars is removed along the Γ–X direction of the PhC [in Fig. 1(c)], a W1-type waveguide is constructed, whose guiding band spans the frequencies of 0.315 a/λ and 0.437 a/λ (1373.00 nm–1904.76 nm), as shown in Fig. 1(d).

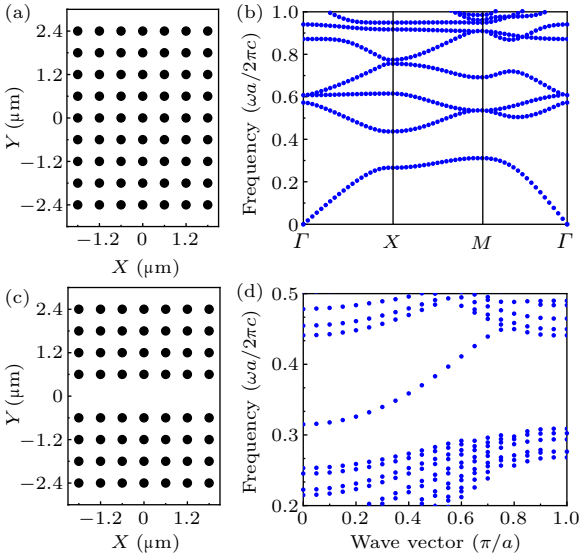


Fig. 1. (a) Schematic geometry of the perfect PhC consisting of AlGaAs pillars immersed in air with a radius of 0.20a. (b) TM-polarized band structure of the PhC. (c) Schematic diagram of the W1-type PhC waveguide. (d) Guiding band of the waveguide.

Based on the above waveguide, we constructed a simple micro-cavity by removing a pillar and keeping its adjacent one and two pillars unchanged on the left and right sides,

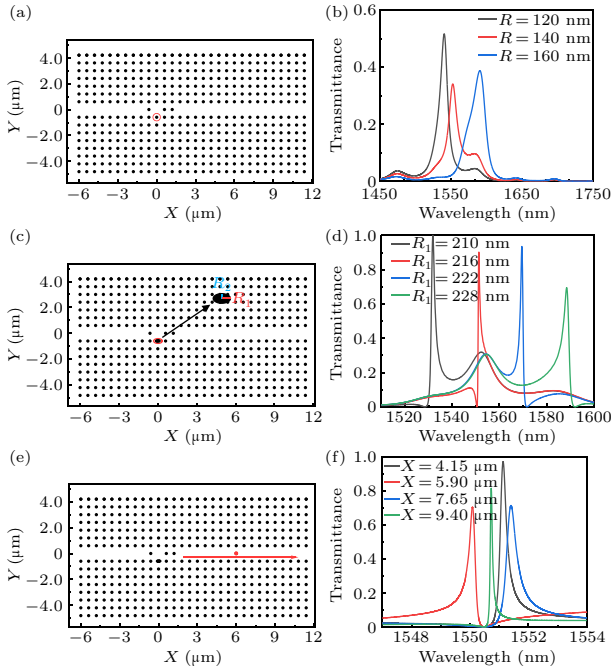


Fig. 2. Structure diagrams and corresponding transmission spectra. (a) Asymmetric micro-cavity with different radius of the pillar circled by the red line. (b) Transmission spectra through the PhC structure at different circular column sizes. (c) Asymmetric micro-cavity with a lateral ellipse shown by the red line. (d) Transmission spectra corresponding to different elliptical long-axis radii R_1. (e) Schematic diagram of a micro-cavity cascaded with a reflection pillar (red dot) in a W1-type waveguide. (f) Transmission spectra corresponding to different positions of the reflector column X.

respectively, as shown in Fig. 2(a). The corresponding transmission spectrum is shown by the black line in Fig. 2(b), where a symmetric transmission peak appears at the wavelength of 1540.26 nm. In addition, two weak transmission peaks exist at the wavelengths of 1472.42 nm and 1582.94 nm. Keeping other structural parameters constant, we changed the radius of the circular pillar (located below the removed column, as indicated by the red curve in Fig. 2(a)) from 120 nm to 140 nm and 160 nm. The corresponding transmission spectra are shown by the red and blue curves in Fig. 2(b), respectively. The transmission peak moves to the longer wavelength as the pillar's size increases, shifting from 1540.26 nm to 1552.37 nm and 1590.53 nm in the case where R is equal to 140 nm and 160 nm. The Q factors of the defective modes are all very small, which is defined by $Q = \lambda_{\text{res}}/\lambda_{\text{FWHM}}$, where λ_{res} is the resonant wavelength of the localized mode and λ_{FWHM} is the full width at half maximum of the transmission peak. To enhance the Q factor of the defect mode, the shape of the pillar mentioned above is changed from a circle to an ellipse, as shown by the red curve in Fig. 2(c). As shown in Fig. 2(b), we calculated the transmission spectra for different long-axis radii R_1, with the short-axis radius R_2 fixed at 120 nm. The black, red, blue, and green curves in the figure represent the long-axis radii of R_1 equal to 210 nm, 216 nm, 222 nm and 228 nm, respectively. This shows that the light transmittance through the elliptical micro-cavity structure is significantly enhanced com-

pared to that of the circular micro-cavity structure. The Fano-resonance between the localized defect mode and the guiding mode of the waveguide also becomes much higher, characterized by the asymmetric transmission peak with higher transmittance and Q factor. This shows that both the transmission peak and valley shift with the alteration of the ellipse's long axis, and the relative location of the transmission peak and valley can also be adjusted. Finally, we introduced a reflective column on the right side of the waveguide to enhance the structural asymmetry for the realization of unidirectional light propagation. The Fano cavity, which contains the nonlinear Kerr medium, is asymmetrically coupled to the F–P cavity (constructed by the micro-cavity and reflective pillar) in the W1-type waveguide, as depicted in Fig. 2(e). Figure 2(f) exhibits the transmission spectra in the case of various reflective column positions, where the transmission peak is sensitive to the alteration of the reflector location, and the transmission valley (reflection peak) remains unchanged.

The AOD is based on the nonlinear Kerr effect that the spatial electric field strength (E_0) at the defect should be somewhat different when light is incident from different directions. According to the formula $\Delta n = n_2 I = \chi^{(3)} |E_0|^2 / n_0$, where n_2 is the Kerr coefficient associated with $\chi^{(3)}$, $\chi^{(3)}$ is the third-order nonlinear coefficient, and I is the intensity of light,[34] the difference in spatial electric field intensity would lead to a difference in refractive index (Δn). This, in turn, would cause the shift of the transmission peak along the long wavelength direction to be inconsistent. This means that the wavelength near the transmission peak could only pass in one direction, thus achieving unidirectional propagation. In the above case, it is known from formula $n = n_0 + \Delta n$ that when the intensity of the pump light increases, the total refractive index of the material (n) will increase, which means that the defect mode will move in the long wavelength direction. Therefore, the pump light intensity is not strong enough to excite the nonlinear Kerr effect of the material when the working wavelength is selected at the trough position, and the AOD maintains in the cutoff state, with the peak of the transmission peak located on the left side of the trough. As the defect mode moves, the optical signal at the working wavelength can be switched from the cutoff state to the propagation state. In order to improve the forward transmission efficiency of the AOD, the transmission spectrum was calculated by adjusting the position of the reflecting column along the horizontal axis (X-axis), and the results are shown in Fig. 3. This shows that when the reflecting pillar is located at $X_1 = 5.8$ μm, the resonant transmission peak is located at the wavelength of 1548.73 nm, with the highest transmittance of 0.99. The Q factor of this mode is 928, and the resonant transmission peak is located at the wavelength of 1550.47 nm with the corresponding transmittance of −57.66 dB. When the reflective pillar's location is changed to 5.9 μm, 6.0 μm and 6.1 μm, the corresponding resonant peaks move to 1550.10 nm, 1550.59 nm and 1550.77 nm, with the transmittance of 0.65, 0.11 and 0.87, and the Q factor of 7045, 3782 and 19384, respectively. It is found that both the wavelength location and transmittance are sensitive to the alteration of the reflective pillar, while the transmission valley remains unchanged. The transmission valley in the four cases shown in Fig. 3 is at 1550.47 nm with the highest transmittance value of −40.14 dB. Therefore, we select the wavelength of 1550.47 nm as the working wavelength.

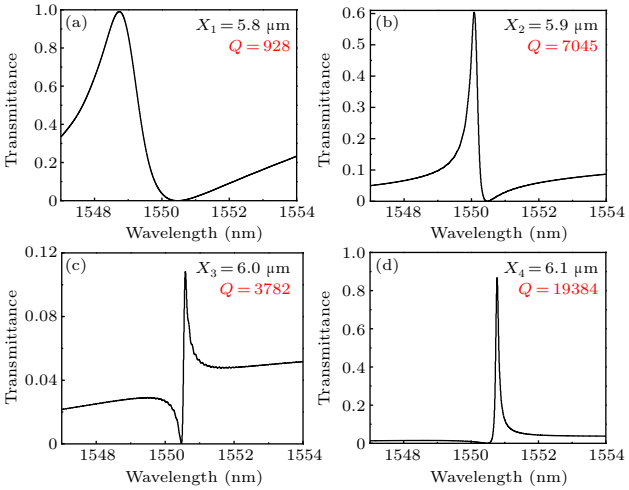


Fig. 3. Transmission spectra through the AOD for the reflecting rod located at different positions. (a) $X_1 = 5.8$ μm. (b) $X_2 = 5.9$ μm. (c) $X_3 = 6.0$ μm. (d) $X_4 = 6.1$ μm.

3. Result analysis

We chose the wavelength of the pump light beam to be 637 nm, which is significantly different from the signal light beam of around 1550 nm and it is also in a higher directional band gap. This means that its main energy can be localized in the waveguide. We change the material of the elliptical column from a perfect dielectric to a nonlinear material, AlGaAs, whose linear refractive index is $n_0 = 3.1$, and $n_2 = 2.1 \times 10^{-12}$ cm^2/W.[33,34] The spatial electric field's amplitudes in the region of the elliptical defect are calculated at the rightwards and leftwards incidences. The ratio of the field amplitudes of the left and right generators reaches 17.86 when $X_1 = 5.8$ μm is pumped with an intensity of 3.97 W/μm^2, while the ratio of the field amplitudes is about 4.75 when $X_2 = 5.9$ μm is pumped with an intensity of 1.13 W/μm^2. We know that the intensity of light is proportional to the square of the amplitude. The intensity of the pump light in the elliptical microcavity is much higher when the pump light is incident to the right side than when it is incident to the left side, showing good unidirectionality. In Figs. 4 and 5, the red curves represent that the signal light and pump light are incident from the left side simultaneously, while the blue curves correspond to the signal light and pump light incident from the right side

of the waveguide. The vertical blue dotted line indicates the optimal incident intensity value, and the vertical orange dotted line represents the location of the working wavelength. The solid black line indicates the normalized power versus time of the pump light, and the black arrows indicate the direction of incidence of the signal and pump light.

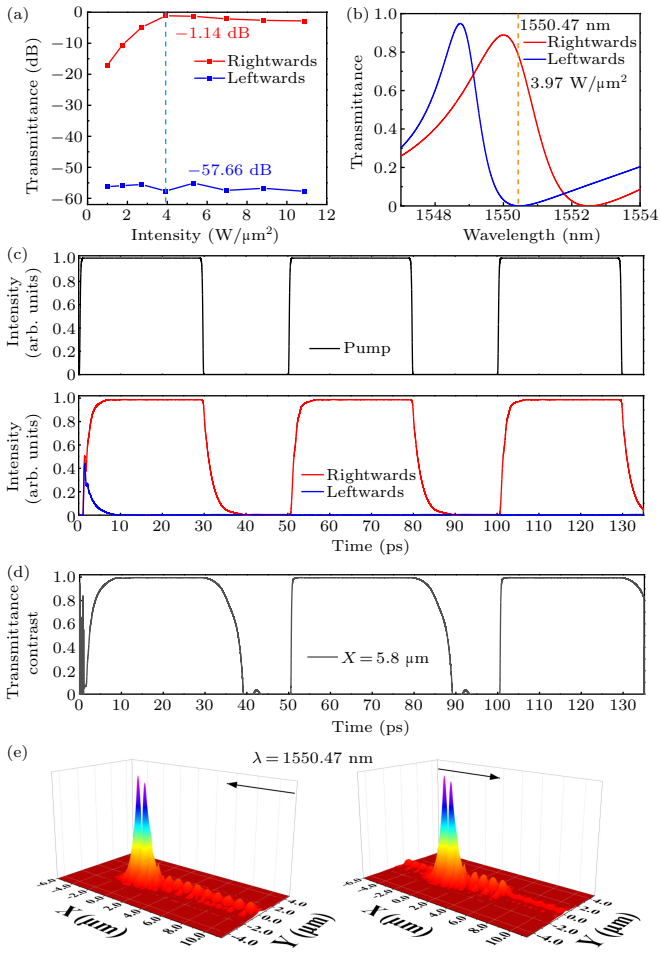


Fig. 4. Coordinate of the AOD for the reflective pillar located at $X = 5.8$ μm. (a) Forward and backward light transmittances influenced by the pump light intensity at the working wavelength of $\lambda = 1550.47$ nm. (b) Light transmission spectra in two opposite propagation directions at the pump light intensity of 3.97 W/μm^2. (c) Time response of the signal light influenced by the alteration of the pump light intensity. (d) Transmission contrast over time. (e) Spatial electric field amplitude distributions when the signal light beam transmits leftwards and rightwards, respectively.

When the X-axis position of the AOD reflective pillar is 5.8 μm, we can see from Fig. 4(a) that transmittance for the light beam traveling rightwards becomes higher with the increase in pump light intensity and achieves a maximum value of −1.14 dB. The lowest transmittance for the signal light incident from the right side is −57.66 dB when the pump light intensity is 3.92 W/μm^2. When the pump light intensity increases further, both the forward and backward transmittances deviate slightly from optimal performance. This indicates that the device can maintain its functionality over a wide range of pump beam intensities. The light transmission curves are calculated for the rightward and leftward incidence cases and the results are shown in Fig. 4(b). Due to the large difference in the light intensity around the nonlinear micro-cavity, the forward transmission peak moves to the location of 1550.00 nm with a transmittance value of 0.889. For the working wavelength of 1550.47 nm, its transmittance is 0.768. In the backward transmission, the transmission peak is located at 1548.74 nm, and the corresponding transmittance is 0.95, almost the same as those without the pump beam. The time response of the signal light beam influenced by the switch of the pump light beam is also studied, and the result is shown in Fig. 4(c). When the pump light of a certain intensity (3.97 W/μm^2) is launched, the signal light incident continuously from the left side of the PhC structure is shifted during propagation in the microcavity region due to the nonlinear material. It eventually propagates to the right side in the waveguide and is detected by the monitor at the right edge of the PhC structure. When the pump light is turned off, the incident signal light propagating both to the right and to the left is blocked, and the time required for the signal light incident to the right to go from on to off is about 10 ps. The transmission contrast C of the all-optical diode is calculated as $C = (T_{\text{Forward}} - T_{\text{Backward}})/(T_{\text{Forward}} + T_{\text{Backward}})$. As shown in Fig. 4(d), this all-optical diode has a high contrast of transmittance under optimal pump light incidence conditions, proving its high efficiency. When the pump light intensity reaches the optimal value, the spatial electric field's amplitude distribution of the signal light transmits rightwards and leftwards, as shown in Fig. 4(e). It is evident that when the light is incident from one direction, it propagates along the W1-type waveguide and is blocked when the light is incident from the other direction.

When the location of the reflective pillar changed to 5.9 μm, the light transmittance and time response influenced by the pump light beam were also studied and the results are shown in Fig. 5. It can be seen from Fig. 5(a) that the value of light transmittance for both the light beam traveling rightwards and leftwards becomes higher with the increase in pump light intensity within the range of 0–1.2 W/μm^2. The maximum value of the transmittance contrast ratio when the pump light intensity is 1.13 W/μm^2, where the forward light transmittance reaches −2.04 dB and the backward transmittance is only −40.14 dB. When the pump light intensity increases further, the forward light transmittance decreases to a small extent and the backward transmittance increases to a much greater extent. Compared to Fig. 4(a), this AOD device works well with a much lower requirement of pump light intensity. Figure 5(b) shows the calculated light transmission curves for the rightward and leftward incidence cases. It shows that the forward transmission peak moves to the location of 1550.47 nm with a transmittance value of 0.62, the transmission valley moves to 1550.94 nm with a transmittance of −40.14 dB. For backward transmission, the transmission peak is located at 1550.10 nm, and the corresponding transmittance is 0.65.

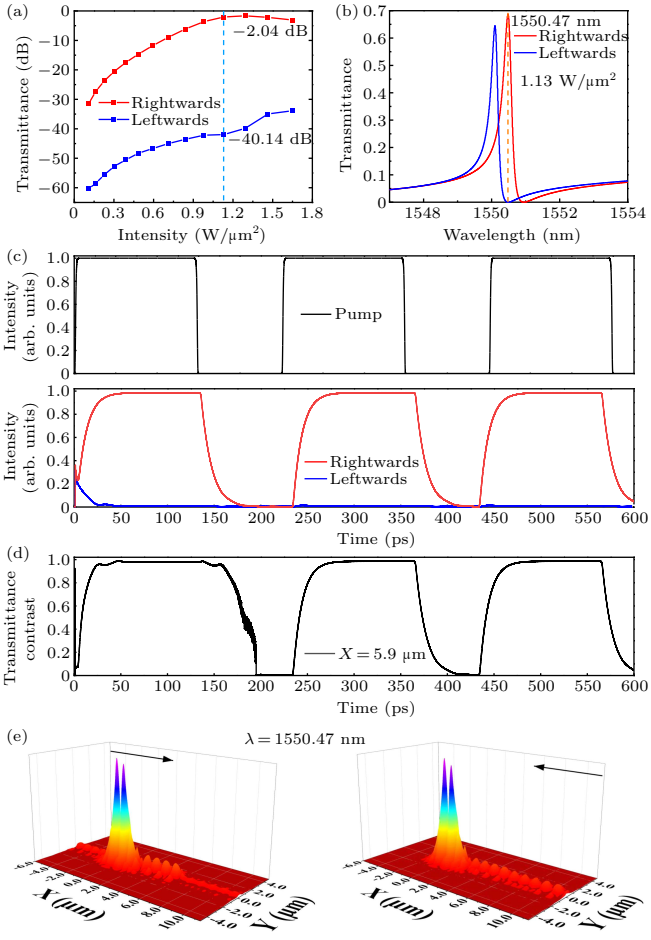


Fig. 5. Coordinate of the AOD for the reflective pillar located at $X =$ 5.9 μm. (a) Forward and backward light transmittance influenced by the pump intensity at the working wavelength of $\lambda = 1550.47$ nm. (b) Light transmission spectra in two opposite propagation directions at the pump light intensity of 1.13 W/μm^2. (c) Time response of the signal light influenced by the alteration of the pump light intensity. (d) Transmission contrast over time. (e) Spatial electric field amplitude distributions when the signal light beam transmits leftwards and rightwards, respectively.

The time response of the signal light beam influenced by the pump light beam's switch is depicted in Fig. 5(c), and it can be inferred that the time required for the signal light beam to reach a stable working status is approximately 50 ps. In Fig. 5(d), the transmission contrast of the all-optical diode is demonstrated under optimal pump light incidence conditions. When the pump light intensity reaches the optimal value, the spatial electric field's amplitude distribution along two opposite incident directions, as shown in Fig. 5(e). It is evident that the light incident from the left can propagate along the W1-type waveguide, while it is cut off for light incident from the right side. Comparing the above two AOD structures, it can be observed that although the structure with the reflective pillar at the X-axis position of 5.8 μm requires higher pump power than the one at 5.9 μm, it offers a higher forward transmission transmittance, a lower reverse cut-off transmittance, and a shorter response time. Therefore, we can choose the PhC structure with the reflective pillar at the X-axis position of 5.8 μm to achieve superior performance, both in the transmittance contrast and quick response time, but a stronger pump light intensity is needed.

4. Conclusion

In summary, we have designed an AOD based on the nonlinear side-coupled elliptical defect and a reflective pillar in the PhC waveguide. The reflective pillar is introduced to construct an F–P cavity with the elliptical defect and to enhance the asymmetric propagation for the signal light traveling rightwards and leftwards, respectively. Through designing the ellipse's size and optimizing the position of the reflective pillar, an AOD device possessing the performance of a quick response time of about 10 ps, a forward light transmittance of −1.14 dB and a reverse cut-off transmittance of −57.66 dB is achieved. Furthermore, our proposed device's size is about 17.4 μm × 9.6 μm. With the advantages of small size, high-transmittance-contrast ratio and short response time, our AOD could be utilized for future all-optical integration.

Data availability statement

The data that support the findings of this study are openly available in Science Data Bank at the following link https://doi.org/10.57760/sciencedb.j00113.00160

Acknowledgments

Project supported by the National Natural Science Foundation of China (Grant Nos. 12274478 and 61775244) and the National Key Research and Development Program of China (Grant Nos. 2021YFB2800604 and 2021YFB2800302).

References

[1] Yablonovitch E 1987 *Phys. Rev. Lett.* **58** 2059
[2] John S 1987 *Phys. Rev. Lett.* **58** 2486
[3] Yablonovitch E, Gmitter T J and Leung K M 1991 *Phys. Rev. Lett.* **67** 2295
[4] Yoel F 1998 *Science.* **282** 1679
[5] Chen B, Li S, Tang T T, Liu C L, Chen H, Li Y D, Huang L and Liu G Z 2011 *J. Light. Technol.* **29** 1975
[6] Wu F, Lu G, Guo Z W, Jiang H T, Xue C H, Zheng M J, Chen C X, Du G Q and Chen H 2018 *Phy. Rev. Appl.* **10** 064022
[7] Wu F, Liu T T and Xiao S Y 2023 *Appl. Opt.* **62** 706
[8] Vujic D and John S 2005 *Phys. Rev. Appl.* **72** 013807
[9] Nozaki K, Shinya A, Matsuo S, Sato T, Kuramochi E and Notomi M 2013 *Opt. Express.* **21** 11877
[10] Zhou J W, Liang J Q, Liang Z Z, Tian C, Qin Y X and Wang W B 2013 *Acta. Phys. Sin.* **62** 134208 (in Chinese)
[11] Chai Z, Hu X Y and Gong Q H 2013 *J. Opt.* **15** 085001
[12] Wang H, Tang G, He Y, Wang Z, Li X, Sun L, Zhang Y, Yuan L, Dong J and Su Y 2022 *Appl. Opt.* **11** 292
[13] Liu K Z, Fan H R, Feng S, Guo H L and Li C B 2019 *Chin. Phys. Lett.* **40** 020501
[14] Jia W, Deng J, Wu H and Li X 2011 *Opt. Lett.* **36** 4077
[15] Din Chai Tee, Kambayashi T, Sandoghchi S R, Tamchek N and Adikan F R M 2012 *J. Lightwave Technol.* **30** 2818
[16] Scalora M, Dowling J P, Bowden C M and Bloemer M J 1994 *J. Appl. Phys.* **76** 2023

[17] Bulgakov E N and Sadreev A F 2014 *Opt. Lett.* **39** 1787
[18] Liu B, Liu Y F, Li S J and He X D 2016 *Opt. Commun.* **368** 7
[19] Sato T, Fujisawa T and Saitoh K 2017 *Opt. Soc. Am. B* **34** 2493
[20] Feng S, Ren C, Wang W and Wang Y 2012 *Europhys. Lett.* **97** 64001
[21] Gallo K, Assanto G, Parameswaran K R and Fejer M M 2001 *Appl. Phys. Lett.* **79** 314
[22] Xie J Y, Hu X Y, Wang F F, Ao Y T, Gao W, Yang H and Gong Q H 2018 *J. Opt.* **20** 034004
[23] Fan C, Shi F, Wu H and Chen Y 2015 *Opt. Lett.* **40** 2449
[24] Cai Z, Shen T, Zhang W and Zheng J 2021 *Opt. Commun.* **484** 126675
[25] Xue C, Jiang H and Chen H 2010 *Opt. Express* **18** 7479
[26] Chen Y, Xu G, Ding Y, Fang Y, Wu X, Wang J and Sun Y 2021 *Opt. Mater. Express* **11** 3275
[27] Fan H, Liu K, Hong X, Feng S, Li C and Guo H 2020 *Appl. Opt.* **59** 4499
[28] Puthiya Purayil N, Kakekochi V, Dalimba U K and Keloth C 2022 *ACS Appl. Electron. Mater.* **4** 138
[29] Chen Z, Li Z and Li B 2006 *Opt. Express* **14** 2671
[30] Liu Y, Qin F, Meng Z M, Zhou F, Mao Q H and Li Z Y 2011 *Opt. Express* **19** 1945
[31] Geerthana S, Syedakbar S, Sridarshini T, Balaji V R, Sitharthan R and Shanmuga Sundar D 2022 *Laser Phys.* **32** 106201
[32] Xu S, Sun Z Z, Wang K, Xiang L, Bao Z, Zhu Z, Shen F, Song Z, Zhang P, Ren W, Zhang X, Dong H, Deng J, Chen J, Wu Y, Tan Z, Gao Y, Jin F, Zhu X, Zhang C, Wang N, Zou Y, Zhong J, Zhang A, Li W, Jiang W, Yu L W, Yao Y, Wang Z, Li H, Guo Q, Song C, Wang H and Deng D L 2023 *Chin. Phys. Lett.* **40** 060301
[33] Espindola R P, Udo M K and Ho S T 1995 *Opt. Commun.* **119** 682
[34] Mobini E, Espinosa D H G, Vyas K and Dolgaleva K 2022 *Micromachines.* **13** 991